Journal of Materials and Environmental Sciences
ISSN : 2028-2508

JMES, 2017 Volume 8, Issue 9, Page 3175-3183

http://www.jmaterenvironsci.com /

Inhibition corrosion of ductile iron by thiadiazol-thiol derivative

Benikdes A.[1] Benali O.[2], Tidjani A.[3], Tourabi M.[4], Ouici H.[5], Bentiss F.[4]

[1]*Department of civil engineering and hydraulic, Faculty of Technology, University of Saïda- Algeria.*
[2] *Department of Biology, Faculty of Sciences, University of Saïda- Algeria.*
[3] *Department of Hydraulics, USTO MB, BP 1505, El Mnaouer, El Mnaouer, Oran 31000 - Algeria.*
[4]*Laboratoire of Catalysis and Materials Corrosion (LCCM), Faculty of Science, University Chouaib Doukkali, El Jadida, Morocco.*
[5]*Department of Chemistry, Faculty of Sciences, University of Saïda, Algeria.*

Received 1 March 2016,
Revised 21 Dec 2016,
Accepted 2 Jan 2017

Keywords
- ✓ Ductile iron,
- ✓ Simulated soil solution,
- ✓ Polarization curve,
- ✓ Inhibition,
- ✓ Corrosion

benaliomar@hotmail.com
Phone: +213662220312

Abstract

Corrosion in drinking water distribution systems can be caused by several factors, including the type of materials used, the age of the piping and fittings, the stagnation time of the water and the water quality in the system, including its pH. The aim of this work is to study the effect of inhibiting the 5-amino-1,3,4-thiadiazole-2-thiol (ATT) on the corrosion of ductile iron in a solution simulating the ground. This study was prepared using electrochemical methods. The results show that the ATT is a good inhibitor in this aggressive environment. The results obtained from the different corrosion assessment techniques are in good agreement. The effect of immersion time, temperature, pH and alkalinity of environment were also studied and the results were discussed.

1. Introduction

Ductile Iron, also known as nodular iron or spheroid-graphite (SG) cast iron, was developed about 50 years ago as a substitute for steel. It contains nodules of graphite embedded in a matrix of ferrite or pearlite or both. The graphite separates out as nodules from iron during solidification because of the additives like cerium (Ce) and magnesium (Mg) introduced into the molten iron before casting [1-2]. These nodules act as crack arresters thereby improving the mechanical properties of ductile iron [3]. The shape of the graphite present in an alloy affects the mechanical properties of the material. Flake graphite acts as a severe stress while the spherodical graphite does not. A classic example of this effect is the difference between gray and ductile cast iron [4-5].
Ductile iron behaviour in corrosive soil under anti-corrosive systems failure for drinking water distribution pipe which supplies the city of Saïda (western Algeria). Corrosion phenomena are generally studied in artificial solutions. The objective is to bring a better comprehension of corrosion damage mechanisms to reduce steel failures in service. Appropriate models for corrosion parameters such as corrosion current density (I_{corr}), corrosion potential (E_{corr}) and polarization resistance (R_p) are used to fit the experimental data and extract the parameters which characterize the corrosion process. We present experimental data obtained by electrochemical measurements on the behaviour of ductile iron in soil simulating solution with and without for 5-amino 1,3,4-thiadiazole 2-thiol (ATT) as corrosion inhibitors by taking cutting sample from the damaged tubes. Soil simulating solution has been chosen a most corrosive soil composition. Corrosion was simulated in laboratory while approaching the industrial context. The effect different parameters such as: temperature, immersion time and NaCl concentration were discussed.

2. Materials and methods

2.1. Study material

Ductile iron (DI) was used as the working electrode for all studies. Samples cover of DI, were obtained from pipe of the Algerian society of water (table 1). Pre-treatment of steels samples surfaces was carried out by grinding with emery paper of 400- 1000 grit, rinsing with bidistilled water and dried at room temperature before us. All tests have been performed at 25, 30, 35 and 40 °C.

Table 1: Chemical Composition of the Ductile Iron Samples

Element	Mn	C	Si	S	P	Mg	Fe
Composition (%)	~ 0.50	~ 3.3	~ 2.4	~ 0.02	~ 0.003	~ 0.05	Balance

2.2. Solution simulating the soil and inhibitor

The corrosion is related to soil conditions in which the structures are buried. The techniques available to determine the aggressiveness of the site may included laboratory test based on a soil chemical analysis in a specific location [6]. Several soil samplings have been taken from various Algerian sites from which we have been chosen the most aggressive composition. Soil extract was prepared according to AFNOR French norm A–05.250 P.278. A mass of soil is taken then mixed with distilled water and analyzed by spectrophotometry microanalysis. The chemical composition of soil is given in table 2. Test solution is obtained by reconstitution of chemical composition of soil in a solution called " the solution simulating soil " (S). Figure 1 shows the molecular structure of the investigated organic compound.

Table 2 - Chemical composition of the solution simulating soil (mg/l)

$CaSO_4$	$MgSO_4$	K_2SO_4	NaCl	Na_2SO_4	$NaHCO_3$
2.00	29.04	1.82	22.69	37.48	0.16

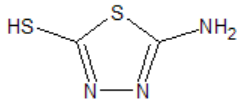

Figure 1. Molecular structure of the investigated 5-ATT

2.3. Electrochemical measurements

Electrochemical measurements were performed in a conventional three-electrode cylindrical Pyrex glass cell. The temperature is thermostatically controlled. DI specimen was used as the working electrode, a platinum electrode as the counter electrode and a saturated calomel electrode (SCE) as the reference electrode. The working electrode (WE) in the form of disc cut from DI has a geometric area of 1.8 cm^2. During each experiment, the test solution was mixed with a magnetic stirrer.

Electrochemical experiments were conducted by using equipment Galvanostat / PGZ potentiostat 100 with controlled Tacussel VoltaMaster 4.

Before each electrochemical experiment, the working electrode was allowed to corrode freely for the considered immersion time and its open circuit potential (OCP) was recorded as a function of time up to 1 h, the time necessary to reach a quasi-stationary value for the open-circuit potential. This steady-state OCP corresponds to the corrosion potential (E_{corr}) of the WE.

For linear polarization resistance (LPR) measurements, the WE was polarised only in the range ±10 mV vs. E_{corr} at a scan rate of 0.167 mV s^{-1}. After studying ac impedance and LPR tests, the potentiodynamic Tafel measurements were scanned from cathodic to the anodic direction, $E = E_{corr} \pm 200$ mV, with a scan rate of 0.5 mV s^{-1}. The Tafel and LRP and CR data were analysed and fitted using the polarization Volatamaster software.

3. Results and discussions

3.1. Potentiodynamic polarization

Potentiodynamic anodic and cathodic polarization curves were carried out at 30 °C in absence and the presence of the inhibitor after 24h of immersion are shown in figure 2.

The polarization parameters values of (I_{corr}), corrosion potential (E_{corr}), polarization resistance, cathodic and anodic Tafel slopes (b_c), (b_a), C.R and the inhibition efficiencies are given in table 4.

The inhibitory efficiency was obtained from equation 1 and 2:

$$EI_{ICORR}\,(\%) = \frac{I_{corr} - I_{corr(i)}}{I_{corr}} \times 100 \qquad (1)$$

where I_{corr} and $I_{corr(i)}$ are the corrosion current density in solutions with and without inhibitor, respectively, determined by extrapolation of Tafel lines (cathode and anode) at the corrosion potential.

and

$$EI_{CR}\,(\%) = \frac{CR - CR_i}{CR} \times 100 \qquad (2)$$

where CR and CR_i are the corrosion rate in solutions with and without inhibitor, respectively, determined by extrapolation of Tafel lines.

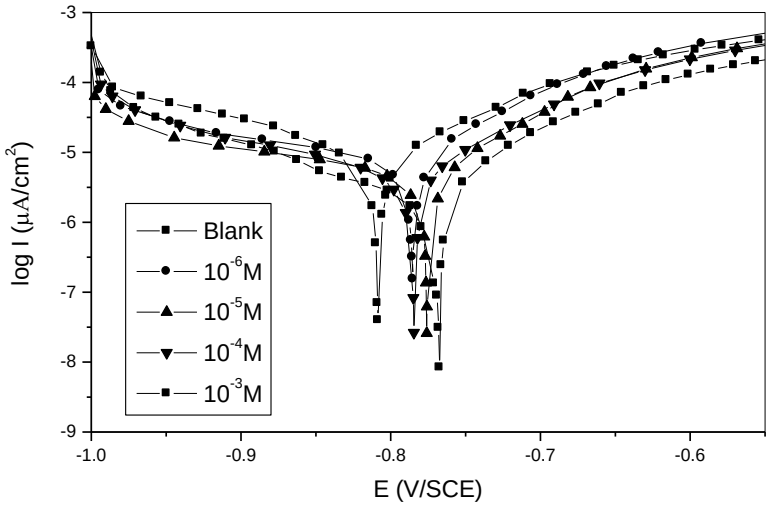

Figure 2. Potentiodynamic polarization curves for DI in (S) at 30 °C and 24h of immersion.

Conc. (M)	$-E_{corr}$ (mV/CSE)	I_{corr} (µA/Cm²)	b_a (mV/Dec)	b_c (mV/Dec)	C.R (µm/Year)	EI_{ICORR} (%)	EI_{CR} (%)
Blank	808	11.67	117	208	136	----	----
10^{-6}	785	5.66	66	110	66.18	**51.50**	**51.34**
10^{-5}	776	4.78	87	250	55.9	**59.04**	**58.90**
10^{-4}	705	4.44	85	166	52	**61.95**	**61.76**
10^{-3}	769	3.33	86	156	39	**71.46**	**71.32**

Table 3. Electrochemical parameters and inhibitory efficiencies for different concentration of ATT after 24 hours of immersion and at 30 °C

Inspection of electrochemical parameters (Table 3) shows that the corrosion current densities decrease with increasing concentration of inhibitor and EI_{ICORR} (%) increases with the concentration of inhibitor up to 71.46%, due to the adsorption of inhibitor molecules to the active sites in the corroded surface [7-8]. It can be seen from the experimental results that the addition of ATT declined significantly I_{corr} for the range of concentrations studied. The presence of ATT has resulted in a shift in the corrosion potential in the anodic direction with respect to the result obtained in the absence of the inhibitor. Both densities anodic and cathodic current decreased, indicating that the ATT blocks both the anodic and cathodic reactions. On the other hand, the values of cathodic and anodic slope are changed in the case of the presence of the inhibitor comparatively of its absence, which indicates that hydrogen evolution and dissolution reactions are not controlled by activation regime [9]. The inhibition efficiencies of ATT obtained by potentiodynamic polarization and by corrosion rate methods are in good agreement.

3.2. Linear polarization resistance (LPR) measurements

Linear polarization technique was performed in aggressive solution with various concentrations of ATT. The corresponding polarization resistance (R_p) values of DI in the absence and in the presence of different inhibitor concentrations are given in Table 4. It is apparent that R_p increases with increasing inhibitor concentration. The inhibition percentage (EI_{RP}%) calculated from R_p values are also presented in Table4. We remark that P% increases with increasing concentration of inhibitor and attains 75.46 %. These results are in reasonably good agreement with the values of inhibitor efficiency obtained from above methods.

The inhibition efficiency of corrosion of DI is calculated by polarization resistance as follows:

$$EI_{Rp}(\%) = \frac{R_p^{'} - R_p}{R_p^{'}} \times 100 \quad (3)$$

where Rp and Rp' are the polarization resistance values without and with inhibitor, respectively.

Table 4: Rp values and the corresponding corrosion inhibition efficiency for the corrosion of DI in (S) at different concentrations of ATT at 30°C

	Rp (kΩ.cm^2)	**EI$_{RP}$ (%)**
Blank	1.06	**------**
10^{-6}	1.94	**45.36**
10^{-5}	2.24	**52.68**
10^{-4}	3.39	**68.73**
10^{-3}	4.25	**75.05**

3. 3. Detailed study of ATT

3.3.1. Effect of immersion time

To assess the stability of the inhibitory behavior of the inhibitor on a time scale, electrochemical measurements were performed in the solution considered in the absence and presence of ATT (10^{-3} M) for the different immersion time temperature 30 °C.

Table 5 shows the efficiency of inhibition against the immersion time. From this table, we can see that the effectiveness of the ATT inhibition increased with the immersion time and then drop after 48 hours of immersion. Increasing the effectiveness of the inhibition is due to the formation of adherent protective film on the metal surface. Increasing values of the effectiveness of the inhibition may be due to the gradual replacement of the water molecules by the adsorption of molecules ATT molecules on the metal surface, which reduces the extent of the dissolution reaction [10].

Table 5. Electrochemical parameters and inhibition efficiency ate different immersion time

Immerssion time (hours)		-E$_{corr}$ (mV/CSE)	I$_{corr}$ (µA/cm^2)	EI$_{ICORR}$%
24	Blank	808	11.67	------
	10^{-3}M	769	3.33	71.46
48	Blank	815	5.18	-----
	10^{-3}M	856	1.36	73.74
96	Blank	802	4.84	-----
	10^{-3}M	817	2.71	44.01

3. 3. 2. Kinetic parameters for inhibitor

The change of the corrosion process rate with the temperature increase was studied in (S), both in the absence and in the presence of 10^{-3} M ATT. We were interested in exploring the apparent activation energy and the pre-exponential factor (A) of the corrosion process. This was carried out by studying the temperature dependence of the corrosion current obtained using potentiodynamic polarisation method.

The various currents densities and the inhibition efficiency were calculated from the polarisation curves and summarised in Table 6. It can be seen from this table that I_{corr} increased with increasing temperature both in uninhibited and inhibited solutions and the values of the efficiency of ATT decreased with temperature in the studied temperature range. The fact that (P%) decrease with temperature is considered as the change in the nature of the adsorption mode, the inhibitor is being chemically adsorbed at lower temperatures, while physisoption is favoured as temperature increases.

Although the adsorption process is well elucidated by a thermodynamic model, a kinetic model is another useful tool to explain the mechanism of corrosion inhibition for the inhibitor.

The corrosion reaction can be regarded as an Arrhenius-type process, the rate is given by :

$$\ln I_{corr} = \frac{-E_a}{RT} + \ln A \quad (4)$$

where E_a represents the apparent activation energy and A is the pre-exponential factor.

Table 6. Variation I_{corr} and the inhibition efficiency according to the temperature.

Temperature (°C)		I_{corr} ($\mu A/cm^2$)	EI_{ICORR}%
30	Blank	11.67	---
	10^{-3}M	3.33	71.46
35	Blank	13.17	---
	10^{-3}M	4.08	69.26
40	Blank	14.14	---
	10^{-3}M	6.51	53.96

Fig. 3 presents the Arrhenius plots of the natural logarithm of the corrosion current density versus $\frac{1}{T}$, without and with addition of 10^{-3} M of ATT.

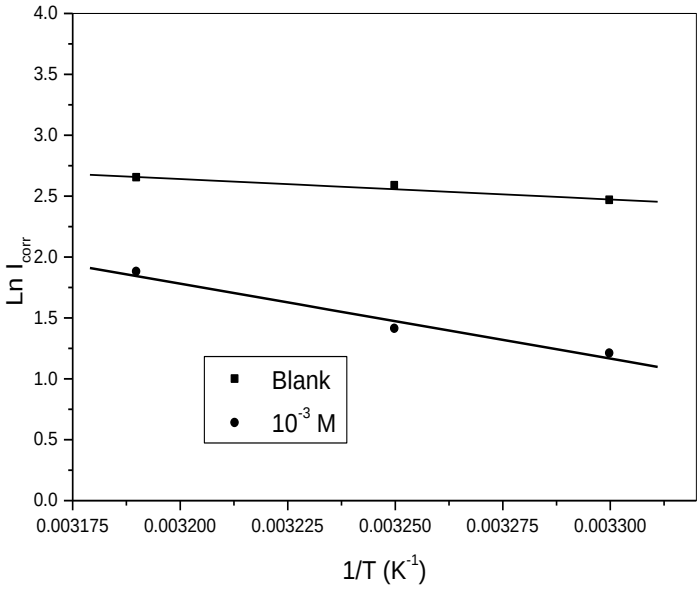

Fig. 3. ln I_{corr} vs. 1/ T for DI dissolution in (S) in the presence of ATT (10^{-3} M)

The apparent activation energies and pre-exponential factor in the absence and in the presence of ATT were calculated by linear regression between ln I_{corr} and $\frac{1}{T}$, and the result is shown in Table 7. All the linear regression coefficient is close to 1, indicating that the ID in (S) can be elucidated using the kinetic model.

Table 7. Some parameters of the linear regression between ln I_{corr} and 1/T

Conc. (M)	Pre-exponential factor ($\mu A\ cm^{-2}$)	E_a ($kJ\ mol^{-1}$)
Blank	1.21×10^5	23.48
10^{-3}	1.34×10^6	32.19

Inspection of data given in Table 7 showed that the activation energy is lower in the presence of ATT than in its absence. According to Eq. (4), it can be seen that the higher pre-exponential factor (A) and the higher E_a lead to the lower corrosion rate. For the present study, the values of E_a in the presence of ATT are higher than those of in its absence. Therefore, the decrease in DI corrosion rate is mostly decided by the pre-exponential factor A. In fact, the value of A significantly increased with the presence of the inhibitor, and the increase in A reduced the

corrosion rate of the iron ductile. So, it is clear that, in this case, the reduction of A is a decisive factor to affect the corrosion rate of DI in the present study.

3. 3. 3 Adsorption considerations

Assuming the corrosion inhibition was caused by the adsorption of ATT on the DI in (S), the degree of surface coverage, θ, of the metal surface was calculated from potentiodynamic polarisation measurements using the following relation [11]:

$$\theta = \frac{I_{corr} - I'_{corr}}{I_{corr}} \quad (5)$$

where I_{corr} and I'_{corr} are the current densities for the blank and the inhibited solutions, respectively.

This equation is valid under the condition of equal slopes of Tafel lines, a condition which is evident in the present work.

The adsorption of an organic adsorbate at a metal solution interface can be represented as a substitutional adsorption process between the organic molecules in the aqueous solution $Org_{(sol)}$ and the water molecules on the metallic surface $H_2O_{(ads)}$ [12].

$$Org_{(sol)} + x\ H_2O_{(ads)} \rightleftharpoons Org_{(ads)} + x\ H_2O_{(sol)} \quad (6)$$

where $Org_{(sol)}$ and $Org_{(ads)}$ are the organic molecules in the aqueous solution and adsorbed on the metallic surface (M), respectively, $H_2O_{(ads)}$ is the water molecules on the metallic surface, *x* is the size ratio representing the number of water molecules replaced by one molecule of organic adsorbate.

According to Bockris and Drazic [13], the inhibition mechanism could be explained by the M-$(inh)_{ads}$ reaction intermediates :

$$M + Inh \rightleftharpoons M(Inh)_{ads} \rightleftharpoons M^{n+} + n\ e + Inh \quad (7)$$

At first, where there is not enough $M(Inh)_{ads}$ to cover the metal surface, because the inhibitor concentration is low or because the adsorption rate is slow, metal dissolution takes place on sites of the DI surface free of $M(Inh)_{ads}$. With high inhibitor concentration, a compact and coherent inhibitor overlayer forms on the DI surface, reducing chemical attack of the metal [14].

When the equilibrium of the process described in Eq. (7) is reached, it is possible to obtain different expressions of the adsorption isotherm plots.

Of the known adsorption isotherm's, the data of θ values were found to fit well with modified Langmuir isotherm. The isotherm is given by:

$$\frac{C}{\theta} = \frac{n}{K} + nC \quad (8)$$

with

$$K = \frac{1}{55,5}\exp\left(-\frac{\Delta G^{0}_{ads}}{RT}\right) \quad (9)$$

where C is the concentration of the inhibitor in the bulk of the solution, K the adsorptive equilibrium constant and $\Delta G°_{ads}$ the free energy of adsorption.

According to this isotherm a plot of $\frac{C}{\theta}$ against C should give a straight line. Fig. 4 shows such these plots at different temperatures, which indicates that the adsorption of inhibitor onto DI accords with the modified Langmuir adsorption isotherm.

The linear regression between $\frac{C}{\theta}$ and C were calculated by the computer, and parameters are listed in Table 8. It can be seen from this table that the adsorption equilibrium constant (K) values increased with increasing temperature, which indicated that ATT was easily adsorbed strongly onto the steel surface at higher temperatures.

Thermodynamic parameters are important to study the inhibitive mechanism. The values of $\Delta G°_{ads}$ at different temperatures were estimated from the values of K and Eq. (11) and plotted against T. This plot is shown in Fig. 5. It should be noted that the entropy change of adsorption $-\Delta S°_{ads}$ is the slope of the straight line $\Delta G°_{ads}$ *vs* T according to equation Eq. (10).

$$\Delta G°_{ads} = \Delta H°_{ads} - T\ \Delta S°_{ads} \quad (10)$$

The intercept of the straight line is used to calculate the heat of adsorption $\Delta H°_{ads}$.

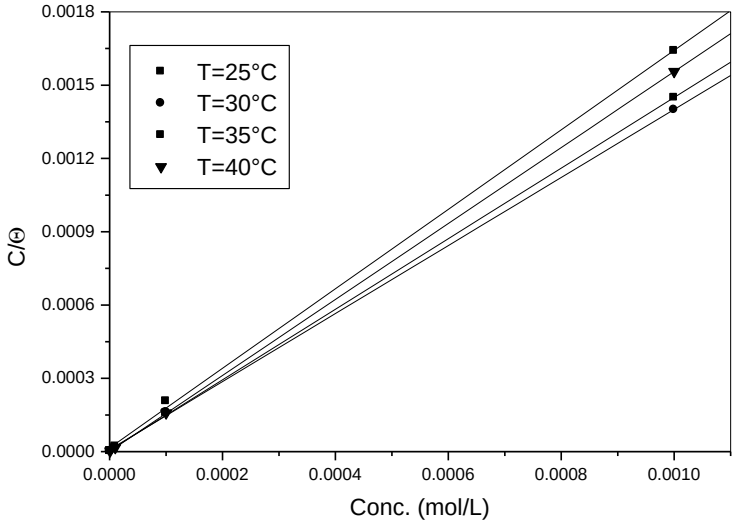

Fig. 4. Curves fitting of the corrosion data of DI in the presence of ATT to Langmuir isotherm at different temperatures.

Table 8. Some parameters of the linear regression between C / θ and C

Temperature (°C)	K (L mol^{-1})	ΔG^0_{ads} (kJ mol^{-1})	Slope
25	1.05 x 10^5	-38.59	1.62
30	1.72 x 10^5	-40.49	1.39
35	3.02 x 10^5	-42.52	1.44
40	7.62 x 10^5	-47.86	1.55

The predicted values of $\Delta H°_{ads}$ and $\Delta S°_{ads}$ are 140.37 kJ mol^{-1} and 598 J mol^{-1} K^{-1} respectively. The large negative values of the free energy of adsorption and the positive value of the heat adsorption are characteristic of the strong adsorption of ATT onto the metal surface. Generally, an exothermic adsorption process signifies either physi- or chemisorption while endothermic process is attributable unequivocally to chemisorption [15]. In the present work, the calculated value of $\Delta H°_{ads}$ for the adsorption of AAT is positive indicating that this inhibitor can be considered chemically adsorbed.

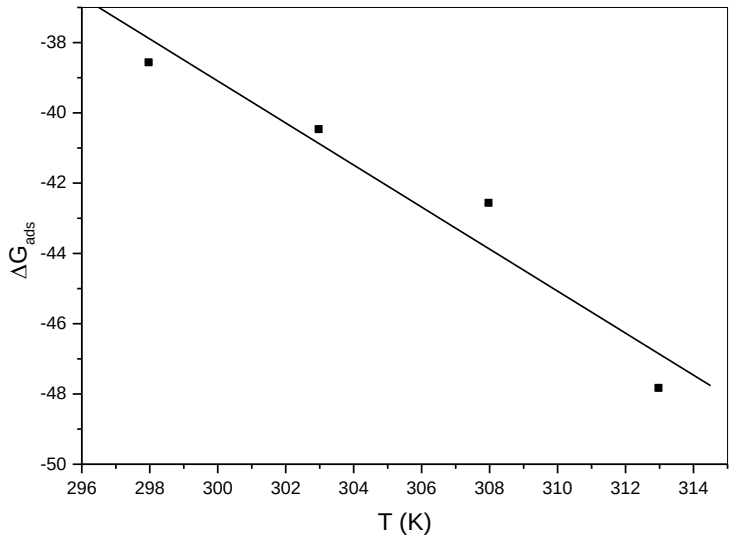

Fig. 5. Free energy of corrosion of cold rolled steel at different temperatures.

Moreover so since both adsorption enthalpy and adsorption entropy are positive values, it can be deduced that the driving force for the adsorption of adsorbate is the increase in entropy during the process of adsorption rather that the decrease in enthalpy.

In the present study, chemisorption is evident from, the apparent activation energy of the corrosion that is lower in presence of ATT than in its absence, the increase in inhibition with temperature, the large negative values of $\Delta G°_{ads}$ and the positive value of $\Delta H°_{ads}$ [16]. According to the above arguments, chemisorption of the ATT molecules on the steel surface, may take place through the donor – acceptor links between the π-electrons of the ring and the empty d-orbitals of the DI atom. ATT can also be adsorbed on the metal surface by the interaction between lone pairs of electrons of nitrogen atoms of the inhibitor and the metal surface.

3. 3. 4. Influence of NaCl concentration

In order to know the influence of the presence of chloride ion on the inhibition efficiency of the compound under investigation, the electrochemical tests were made at various concentrations of NaCl (1% and 2%). The polarization parameters values of I_{corr} and inhibition efficiency are given in table 9.

Table 9. Values of I_{corr} and inhibition efficiency of ATT in presence of NaCl after 24 h of immersion and 30°C

	NaCl 1%		**NaCl 2%**	
Conc. (Mol/L)	I_{corr} (µA/cm^2)	EI (%)	I_{corr} (µA/cm^2)	EI (%)
Blank	20.9	----	14.12	-----
10^{-6}	13.18	**36.94**	6.60	**52.26**
10^{-5}	6.91	**66.94**	6.16	**56.37**
10^{-4}	6.30	**69.86**	5.37	**61.97**
10^{-3}	3.63	**82.63**	4.07	**71.17**

From this table we clearly notice the corrosion currents decrease with increasing concentrations of ATT, on the other hand, the values of I_{corr} in blank solutions are strangely affected by the presence of Cl^-. The EI_{ICORR} (%) increases with the concentration of inhibitor up to 82.63% in the presence on NaCl 1% and 71.17% for 2% of NaCl.

The synergetic effect of this halide ion with ATT may be due to co-adsotrption of Cl^- and ATT molecules which may be either competitive or cooperative [17]. In competitive adsorption the Cl^- and ATT are adsorbed at different sites on the metal. In cooperative adsorption the Cl^- is chemisorbed on the surface and molecule is adsorbed on a layer of the anion [18].

Conclusions

This paper studies the effect of the addition of 5-amino-1,3,4-thiadiazole-2-thiol (ATT) on the corrosion of ductile iron in a solution simulating the soil. The electrochemical methods were used to evaluate the inhibition efficiency of this compound in function of immersion time, temperature and chloride content.

The results obtained from the different corrosion assessment techniques are in good agreement. The influence of the immersion time shows that the ATT is more effective for 24 hours and 48 hours. The obtained results, show that the ATT it is effective at low temperatures and that chemically adsorbed. The influence of the presence of chloride ion shows that the addition of NaCl 1% increased the efficiency considerably.

References

1. Aver S.H., (1974); Introduction to physical metallurgy second edition McGraw-Hill Publishers, London pp: 146.
2. Prasanna N. D. (2000); Effect of processes variables on the structure mechanical properties and wear characteristics of Austempred Ductile Iron, Ph.D thesis, Bangalore University, March 2000.
3. Allen D.K., (1983); Metallurgy theory and practice, American technical society Chicago.
4. Aramide F.O., Olorunniwo E.O., Atanda P.O., Borode J.O., *J. Miner. Mater. Charact. Eng.*, 9 (10) (2010) 867-877.

5. ASTM Annual Book "Standard Specification for Automotive Gray Iron Casting ", A159-83, Vol. 0.1-0.2, (1986).
6. Belmokre K., Azzouz N., Kermiche F., Wery M. and Pagetti J., *Mater. Corros.*, 49 (1998) 108.
7. Landolt D., Corrosion Metals Surface Chemistry, Alden Press, Oxford, 1993, p. 495.
8. Larabi L., Harek Y., Benali O.and Ghalem S., *Prog. Org. Coat.*, 54 (2005) 256.
9. Benali O., Larabi L., Tabti B., Harek Y., *Anti-Corros. Met. and Mat.*, 52 (2005) 280.
10. Benali O., Ouazene M., *Arab. J. Chem.*, 4 (2011)443.
11. Gomma G. K., *Mater. Chem. Phys.* 55 (1998) 131.
12. Bockris J. O'M, Swinkels D. A. J., *J. Electrochem. Soc.* 111 (1964) 736.
13. Bockris J. O'M, Drazic D., *Electrochim. Acta* 7 (1962) 293.
14. Branzoi V., Branzoi F., Baibarac M., *Mater. Chem. Phys.* 65 (2000) 288.
15. Ghazoui A., Benchat N., El-Hajjaji F., Taleb M., Rais Z., Saddik R., Elaatiaoui A., Hammouti B., *Journal of Alloys and Compounds*, 693 (2017) 510-517
16. El-Hajjaji F., Belkhmima R.A., Zerga B., Sfaira M., Taleb M., Ebn Touhami M., Hammouti B., Al-Deyab S.S., Ebenso E.E., *Int. J. Electrochem. Sci*., 9 (2014) 4721 - 4731
17. Asefi A., Arami M., Sarabi A. A., *ECS Transactions* 19(29) (2009) 135.
18. Jeyaprabha C., Sathiyanarayanan S., Venkatachari G., *Electrochim. Acta*, 51 (2006) 4080

(2017) ; http://www.jmaterenvironsci.com